Ocean Modelling xxx (2013) xxx–xxx

Contents lists available at SciVerse ScienceDirect

Ocean Modelling

journal homepage: www.elsevier.com/locate/ocemod

A global wave parameter database for geophysical applications. Part 2: Model validation with improved source term parameterization

Nicolas Rascle [a,b,*], Fabrice Ardhuin [a]

[a] Laboratoire d'Océanographie Spatiale, Institut Francais de Recherche pour l'Exploitation de la Mer, Plouzané, France
[b] Nansen-Tutu Center, Department of Oceanography, University of Cape Town, Rondebosch, South Africa

ARTICLE INFO

Article history:
Available online xxxx

Keywords:
Waves
Hindcast
Air–sea fluxes
Stokes drift
Mean square slope
Seismic noise

ABSTRACT

A multi-scale global hindcast of ocean waves is presented that covers the years 1994–2012, based on recently published parameterizations for wind sea and swell dissipation [Ardhuin, F., Rogers, E., Babanin, A., Filipot, J.-F., Magne, R., Roland, A., van der Westhuysen, A., Queffeulou, P., Lefevre, J.-M., Aouf, L., Collard, F., 2010. Semi-empirical dissipation source functions for wind-wave models: Part I. Definition, calibration and validation. J. Phys. Oceanogr. 40 (9), 1917–1941]. Results from this hindcast include traditional wave parameters, like the significant wave height and mean periods, and we particularly consider the accuracy of the results for phenomenal sea states, with significant heights above 14 m. Using unbiased winds, there is no evidence of a bias in wave heights even for this very high range. Various spectral moments were also validated, including the surface Stokes drift and mean square slopes that are relevant for wave–current interactions modelling and remote sensing, and also spectra of seismic noise sources. The estimation of these parameters is made more accurate by the new wave growth and dissipation parameterizations. Associated air–sea fluxes of momentum and energy are significantly different from what is obtained with the WAM-Cycle 4 parameterization, with a roughness that is practically a function of wind speed only. That particular output of the model does not appear very realistic and will require future adjustments of the generation and dissipation parameterizations.

© 2012 Elsevier Ltd. All rights reserved.

1. Introduction

Numerical wave models have traditionally been calibrated mostly in terms of wave heights, and to a lesser extent peak periods and directions. However, new applications require the validation of air–sea fluxes (e.g., Moon et al., 2004), higher order spectral moments such as the surface Stokes drift and mean square slopes (e.g., Tran et al., 2010), and spectral shape that controls the second order spectrum which is responsible for driving long waves and generating seismic noise (e.g., Reniers et al., 2010; Ardhuin et al., 2011b). Physical parameterizations have been proposed recently that capture some of the variability of the high frequency spectral levels, and these also lead to more accurate results for the dominant waves. Based on this experience, we expect that improvements for specific applications will generally lead to benefits for all users of numerical wave models. Also, the validation of many different parameters estimated from wave spectra may also provide some constraints on the otherwise 'free parameters' that are still too many in wave generation and dissipation parameterizations. Among these, wave breaking statistics may be used to constrain the parameterization of wave dissipation (Banner et al., 2000; Leckler et al., 2011), but breaking statistics require a detailed discussion that will be presented elsewhere. At the very least, our goal is to document the impact of the parameterizations on important model results, such as the air–sea fluxes. In particular the parameterization proposed by Ardhuin et al. (2010) is now used operationally at the French Weather Service (Meteo-France) since 2011 and, with its latest adjustment described below, at the US Weather Service (NOAA/NCEP) since May 2012. The associated wave products are thus likely to be widely used by a large range of users which should know what to expect.

For this purpose, we have generated an accurate and homogeneous series of wave hindcasts, also valid for extreme events. This has led us to limit the time frame of our hindcast to the years after 1993. All the results are freely available at http://tinyurl.com/iowagaftp/HINDCAST (see Appendix A for a description of the data, output parameters and conventions).

In a previous paper, Rascle et al. (2008) hereinafter Part 1 presented a first wave hindcast of wave parameters with an emphasis on air–sea flux parameters. That hindcast was obtained with older parameterizations. Following this work, the aim of the present paper is to highlight the improvements and the limitations of the

* Corresponding author. Address: IFREMER/LOS, Z.I. Pointe du Diable, 29280 Plouzané, France. Tel.: +33 2 98 22 45 54; fax: +33 2 98 22 45 33.
E-mail address: nicolas.rascle@ifremer.fr (N. Rascle).

1463-5003/$ - see front matter © 2012 Elsevier Ltd. All rights reserved.
http://dx.doi.org/10.1016/j.ocemod.2012.12.001

Please cite this article in press as: Rascle, N., Ardhuin, F. A global wave parameter database for geophysical applications. Part 2: Model validation with improved source term parameterization. Ocean Modell. (2013), http://dx.doi.org/10.1016/j.ocemod.2012.12.001

new wave hindcasts database. We thus give details about those new hindcasts, which have been produced with two different and widely used wind reanalysis. We compare those new hindcasts with the hindcast obtained with older parameterizations and discussed in Part 1. We document and validate the improvement against observations of both low-order (wave height, peak period, direction) and high order spectral moments (mean square slope, Stokes drift). We also document the consequences in terms of physical quantities more difficult to validate with observations, such as seismic noise sources and air–sea energy and momentum exchange. That latter part in particular might help to drive future developments of wave modelling for geophysical applications.

The paper is organized as follows. The model settings and forcing fields are described in Section 2. Results in terms of dominant wave parameters are presented in Section 3 and in terms of wave directionality and seismic noise sources in Section 4. Discussion of the associated air–sea energy and momentum exchange follows in Section 5 and conclusions in Section 6.

2. Model set-ups

2.1. Model grids and parameterizations

The wave hindcasts presented here are all based on the WAVEWATCH III^R model in its version 4.04. A first baseline simulation was performed with a single grid at 0.5° resolution in longitude and latitude, using a spectral grid with 24 directions and 31 frequencies exponentially spaced from 0.037 Hz to 0.7 Hz. This was complemented by a multi-grid system (Tolman, 2008) that include that same grid and higher resolution along the North American coasts and Europe, around French Polynesia and Hawaii, at 10′ resolution, at the West Indies and New Caledonia at 3′ resolution. The Quickest third order scheme is used together with garden sprinkler reduction (Tolman, 2002). The spectra from this multi-grid system have been used to force stand-alone coastal domains using unstructured grids that are using the residual distribution Narrow stencil scheme adapted by Roland (2008). For the sake of demonstration, we have particularly focused on the West coast of France, in the Iroise sea, taking the grid already used by Ardhuin et al. (2009, 2012), with a 100 m spacing along the coast. This high-resolution dataset has already been used for coastal geomorphology applications (Fichaut and Suanez, 2011; Suanez et al., 2012).

All models use a new parameterization called TEST451 for wind wave generation and dissipation. That parameterization has been described[1] in details in Ardhuin et al. (2010). Its main features are

- Following Tolman and Chalikov (1996), a well separated dissipation of swell (negative wind input) and dissipation due to breaking.
- A non-linear swell dissipation based on SAR-derived dissipation rates across the Pacific (Ardhuin et al., 2009).
- Following Phillips (1984), a breaking-induced dissipation that is based on the local saturation spectrum. Here the saturation is integrated over a wide angular sector but not the full circle, which leads to a higher dissipation rate in the mean wave direction. That particular aspect was designed to fit observed directional spreadings.
- A cumulative dissipation rate inspired by Babanin and Young (2005) but directly estimated from breaking wave probabilities. This dramatically enhances the dissipation at frequencies above three times the peak frequency.
- A reduced wind input at high frequencies compared to Janssen (1991), and an intermediate input level at the peak, compared to the higher values with Janssen (1991) and much lower values with Tolman and Chalikov (1996). This effect is parameterized as a sheltering term, reducing the effective winds for the shorter waves (Chen and Belcher, 2000; Banner and Morison, 2010).
- The discrete interaction approximation (Hasselmann et al., 1985) for the non-linear interactions.

That last approximation is well known to be inaccurate, and the dissipation source terms are usually used to compensate for its errors (Banner and Young, 1994; Ardhuin et al., 2007). We note that the model was run with 10-m winds, without any air–sea stability correction. Absolutely no wave measurement, direct or indirect, was assimilated in the model. In contrast, many observations from satellite altimeter and SAR to buoys were used to calibrate the model parameters over the year 2008 (Ardhuin et al., 2010).

2.2. Forcing fields

The models were forced by winds from the Climate Forecast System Reanalysis (Saha et al., 2010) hereinafter CFSR. For years 2005 to the present we also used ECMWF (European Centre for Medium-Range Weather Forecasts) operational analyses from their Integrated Forecast System. Another forcing is the sea ice cover, which is taken from the CFSR reanalysis when using CFSR winds, or the ECMWF analysis when using ECMWF winds. These ECMWF ice concentrations actually come from the EUMETSAT Ocean and Sea Ice Satellite Application Facility (OSI/SAF). For the years 2003–2010, iceberg statistics for the Southern Ocean have been derived from altimeter data using the method by Tournadre et al. (2008, 2012) and incorporated in the global model following the method by Ardhuin et al. (2011b). As a result of our forcing choices, the hindcasts contain some discontinuities in the Southern Ocean, due to the effects of icebergs. This will be corrected after an ongoing effort to reprocess ERS and TOPEX altimeter data for obtaining iceberg statistics.

The reason for using the two wind fields, CFSR and ECMWF, is that each dataset has some advantages. Namely, the ECMWF analysis typically yields smaller random errors for wave parameters for years after 2005, compared to CFSR winds. This smaller random error is interesting for verifying the reduction in random errors associated with our use of new parameterizations for wave generation and dissipation. However, ECMWF winds produce a strong negative bias for large wave heights. This different behavior can be traced to the different distributions of wind speeds in these two datasets (Fig. 1).

Given the large bias between the two data sets, we adjusted the wind-wave growth parameter from $\beta_{max} = 1.52$ with ECMWF winds, to $\beta_{max} = 1.33$ for CFSR winds (see Eq. (19) in Ardhuin et al., 2010). This adjustment was calibrated for the year 2008 and was found to give good results for the years 1994 to 2009. That is the only adjustment done to the model when the source of wind forcing is changed.

2.3. Summary of the model runs

In this paper the results obtained with the new parameterization TEST451 will be compared to those obtained with the parameterization by Bidlot et al. (2005), hereinafter BJA, that was used in Part I (Rascle et al., 2008). The use of different wind forcings will also be evaluated.

For the purpose of coherent comparisons, three model runs have thus been performed, two using the model with the new parameterization TEST451 and forced with two different wind fields, CFSR and ECMWF, and one run with the model with the

[1] The parameterization actually described in Ardhuin et al. (2010) is version TEST441b. The version TEST451 used here is similar but includes a minor recent modification to improve the swell dissipation (see Appendix B).

Please cite this article in press as: Rascle, N., Ardhuin, F. A global wave parameter database for geophysical applications. Part 2: Model validation with improved source term parameterization. Ocean Modell. (2013), http://dx.doi.org/10.1016/j.ocemod.2012.12.001

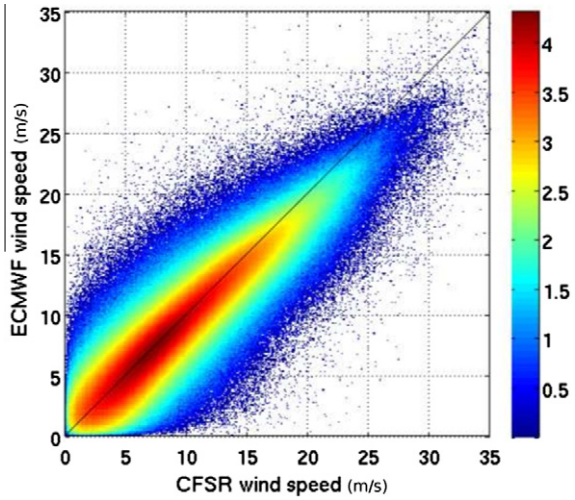

Fig. 1. Dispersion of CFSR versus ECMWF analyses for the month of January 2005. The color scale is the base-10 logarithm of the number of data points in each 0.1 m/s bin.

Table 1
The three different model runs compared in this paper.

Hindcast name	TEST451 CFSR	TEST451 ECMWF	BJA
Parameterization	TEST451 Ardhuin et al. (2010)	TEST451 Ardhuin et al. (2010)	BJA Bidlot et al. (2005)
Forcing	CFSR	ECMWF	ECMWF
β_{max}	1.33	1.52	–
Period	1994–2012	2005–2012	2005–2012

BJA parameterization forced with ECMWF winds. This is summarized in Table 1.

3. Dominant wave parameters and spectral moments

3.1. Effects of the different wind forcing on extreme wave heights

In this paragraph, the model with the new parameterization TEST451 is forced with the two different wind forcings. Due to a different shape in the distributions of high winds, shown in Fig. 1, the ECMWF and CFSR winds produce different biases in different ranges of the wave heights. Interestingly, the strength of high winds in CFSR, compared to ECMWF analysis, reduces the negative bias for very high ($H_s > 9$ m) and phenomenal ($H_s > 14$ m) seas (Fig. 2a, compare blue squares to black crosses), and allows a remarkable reduction in root mean square (rms) errors for the highest waves, even though the random errors are larger in 2008 when using CFSR winds (Fig. 2b). This finding is consistent with a detailed analysis of the 14 February 2011 North Atlantic storm which produced significant wave heights up to 20 m (Hanafin et al., 2012).

The model errors are compared using a normalized root mean square error (NRMSE),

$$\mathrm{NRMSE}(X) = \sqrt{\frac{\sum (X_{\mathrm{obs}} - X_{\mathrm{mod}})^2}{\sum X_{\mathrm{obs}}^2}} \quad (1)$$

and a scatter index (SI), which is the same thing for non-biased quantities,

$$\mathrm{SI}(X) = \sqrt{\frac{\sum \left[(X_{\mathrm{obs}} - \overline{X_{\mathrm{obs}}}) - (X_{\mathrm{mod}} - \overline{X_{\mathrm{mod}}})\right]^2}{\sum X_{\mathrm{obs}}^2}} \quad (2)$$

where X is any quantity, and the overbar denotes the arithmetic average. The SI, which represent the random errors, are shown in Fig. 2b.

One of the difficulties in producing long-term wave hindcasts is the consistency of the wind forcing in time, and, if possible, to correct for its biases. This was addressed by Caires et al. (2004) for the ERA-40 reanalysis, and Reguero et al. (2012) for the NCEP/NCAR reanalysis. In the case of CFSR winds, some time-varying biases are discussed here and have also been analyzed by Cox et al. (2011) and Chawla et al. (2012). In our model results with the CFSR wind forcing, the spatial pattern of biases for the significant wave height is fairly constant for the years 2003 to 2010 for which we have used a masking by small icebergs (Ardhuin et al., 2011c). For the years 1991 to 2001, Fig. 3 shows that there is a 2% bias shift for the years 1994, 1995, 1998, 1999 compared to 1996, 1997, 2000 and 2001. But more importantly, it reveals a very strong anomalous bias (about 10%) for the years 1991 to 1993.

This bias can be seen both in altimeter data, at the global scale, and in buoy data from the US coast, in particular at the 46211 buoy, operated by CDIP. At that buoy the model bias exceeds 17% for H_s for these years, compared to approximately 3% for the years 2004–2008 (not shown).

The examination of CFSR winds and waves compared to altimeter data shows that the errors are strongest over the Southern Ocean (not shown) and disappear in 1994. Chawla et al. (2012) have analyzed this bias and have rather interpreted it as an increase in extreme values of the wind speed. Instead, (Ardhuin et al., 2011a, see their Fig. 3) have shown that even the mean values are strongly biased, up to 1 m/s, but this bias is confined to latitudes south of 30 degrees South. Looking at the details of the data assimilated into CFSR, we can see that 1994 corresponds to the start of SSM-I wind speed assimilation (Fig. S14 in Saha et al. (2010)). It thus appears that SSM-I data has a beneficial impact, reducing the high bias of high winds in the sub-polar regions. So far we have left the 1991-1993 results uncorrected. It is possible that a correction of the CFSR wind speed histogram may be enough to correct the biases on wave parameters.

For the years before 1991, in the absence of global validation data from satellite altimeters, it is difficult to guarantee the stability of biases for the modelled wave parameters. This will be investigated further using seismic noise data (Ardhuin et al., 2011b, 2012). In order to limit the scope of the present paper we have thus chosen to start our hindcast in 1994. There are still some issues with CFSR winds in later years. These are very well discussed by Chawla et al. (2012), with an increase of the extreme wind speeds for the years 2006 to 2009. This can be seen also in our Fig. 3. However, these winds still provide consistent wave parameters.

In the case of the operational analyses from ECMWF, which we used from 2005 to 2012, there is also an increasing positive bias in 2011 and 2012 in the Southern Ocean compared to the previous years. For these reasons we have chosen to illustrate the comparison of ECMWF and CFSR winds using the year 2005, at a time when their random errors are comparable. Because some of the validation data that we use is only available for later years, we have also used model runs with ECMWF winds for the year 2008.

3.2. Improvement of wave heights with the new parameterization

As already shown in Ardhuin et al. (2010) the wave heights obtained with the new parameterization TEST451 have much smaller biases than those obtained with the parameterization BJA in part I, typically now ranging from −20 cm in the Central Tropical Pacific, to +30 cm in parts of the Southern Ocean (Fig. 4a). We note that such biases are also much smaller than those obtained with the parameterization by Tolman and Chalikov (1996) used by Chawla

Please cite this article in press as: Rascle, N., Ardhuin, F. A global wave parameter database for geophysical applications. Part 2: Model validation with improved source term parameterization. Ocean Modell. (2013), http://dx.doi.org/10.1016/j.ocemod.2012.12.001

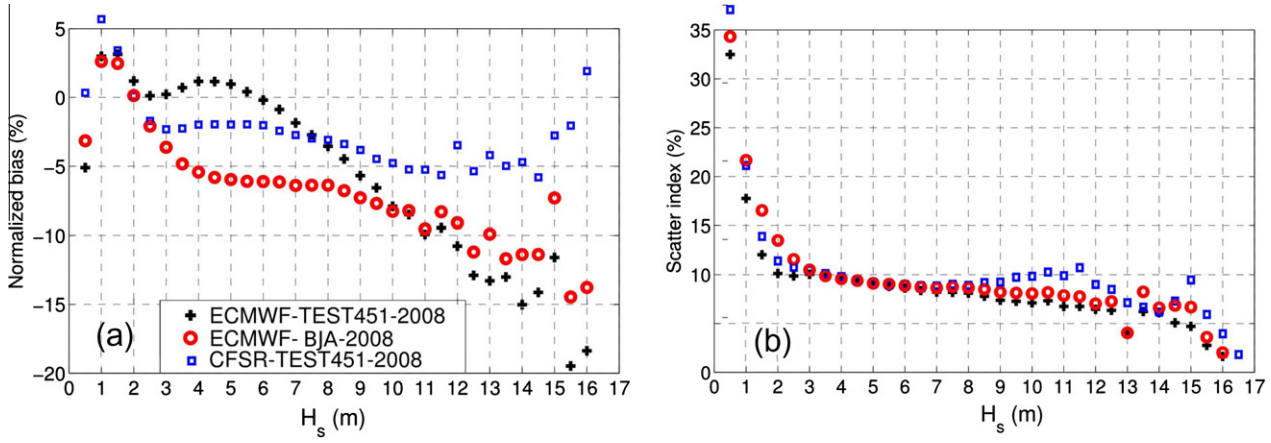

Fig. 2. (a) Normalized bias and (b) scatter index for H_s in 2008, against altimeter data, as a function of H_s, for different wind forcings (ECMWF or CFSR) and parameterizations (TEST451 or BJA). In this case we use a single grid of 0.5 degree resolution.

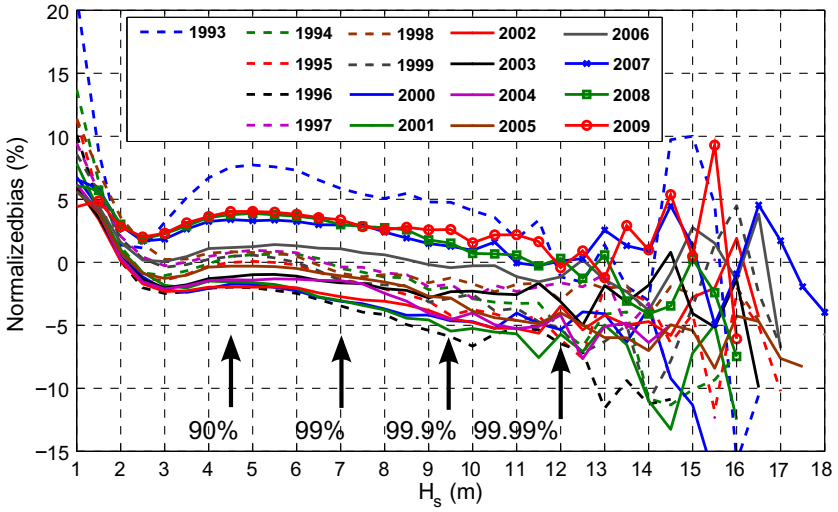

Fig. 3. Normalized bias for H_s against altimeter data, as a function of H_s, for the years 1993 to 2009. The new parameterization TEST451 is used with the CFSR wind forcing.

et al. (2012). This reduced bias is largely due to the swell dissipation parameterization, which is the single most sensitive part of the model. Indeed a change of the swell dissipation coefficient by 10% typically gives a change of global wave heights by 30 cm on average.

This improvement is also illustrated by the large reduction in bias and random error for wave heights under 3 m when the BJA parameterization is replaced by TEST451 (Fig. 2b, compare black crosses to red circles).

Both biases and random errors for the year 2009 are very similar to the results shown for the year 2007 in Ardhuin et al. (2010), with an additional significant reduction in random errors in the central Pacific (Fig. 4b), associated with the smoothing of the swell dissipation threshold (see Appendix B).

In general the random errors are lowest, below 8%, in the trade wind areas between 5 and 20 degrees of latitude, where winds are usually very steady. The largest random errors are found in semi-enclosed basins, usually associated with low biases. This is partly the result of larger wind errors there but is also associated with a low bias at short fetch in the TEST451 parameterizations, already documented by Ardhuin et al. (2010) and Filipot and Ardhuin (2012).

3.3. The mean square slopes

Either from model or satellite altimeter, the estimates of the mean square slope (mss) are indirect but they provide an interesting check on the variability of the spectral tails, which is very much controlled by the cumulative dissipation term (e.g., Leckler et al., 2011).

For linear waves the mss is proportional to the acceleration variance, which is the fourth moment of the wave spectrum. One could thus estimate a fourth moment mean period $T_{m0,4}$ from H_s and mss. We note that several groups have also developed empirical algorithm to estimate the second moment mean period, T_{m02} from H_s and the radar cross section (Gommenginger et al., 2003). However, the empirical nature of these algorithms naturally limits their validity and we prefer to verify the model with the mss which is more directly measurable.

We thus estimate a mss from Ku band cross section as

$$\mathrm{mss}_{\mathrm{Ku}} = \frac{0.48}{\exp\left[(\sigma_0 + 1.4) \times (0.1 \log(10))\right]}, \tag{3}$$

where σ_0 is the normalized radar cross section as provided in the Globwave homogenized dataset (Queffeulou and Croizé-Fillon,

Please cite this article in press as: Rascle, N., Ardhuin, F. A global wave parameter database for geophysical applications. Part 2: Model validation with improved source term parameterization. Ocean Modell. (2013), http://dx.doi.org/10.1016/j.ocemod.2012.12.001

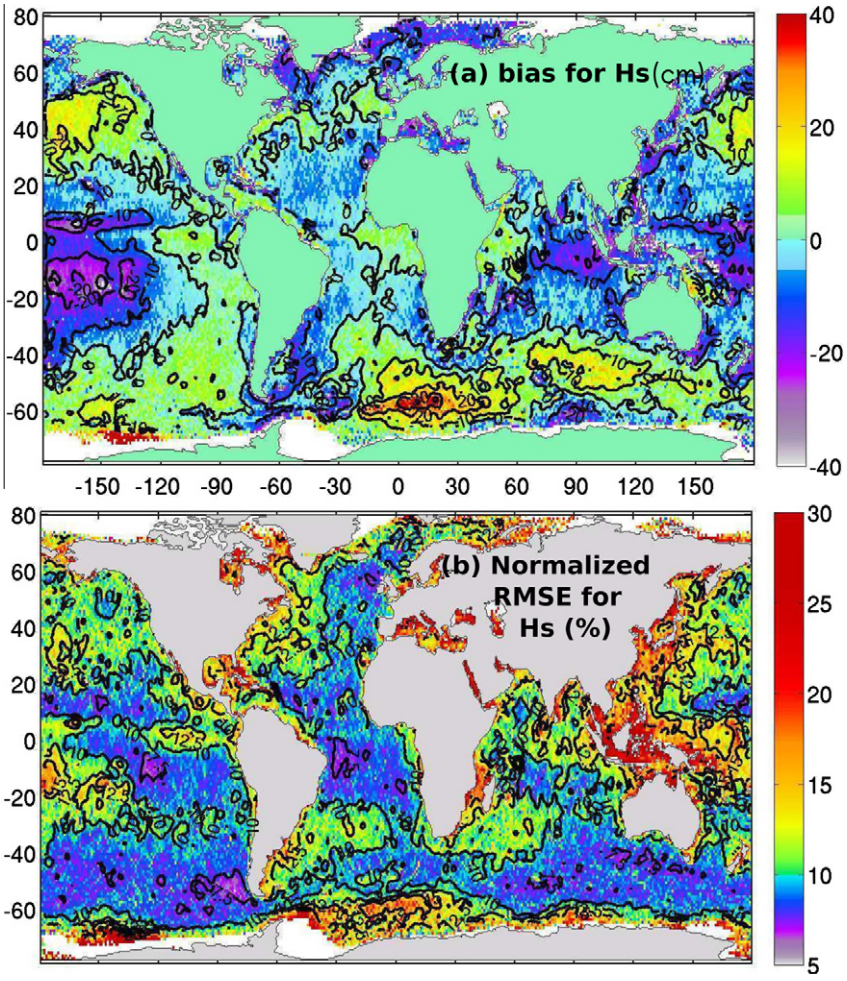

Fig. 4. (a) Bias and (b) normalized RMS error for the modelled significant wave heights for the year 2005, against data from Jason-1, Jason-2 and Envisat altimeters. The new parameterization TEST451 is used with the CFSR wind forcing. Both model and altimeter data are averaged along the satellite tracks over 1 degree in latitude. There are 2.4 million averaged values.

2010), 1.4 is a bias correction in dB, and 0.48 is an effective Fresnel coefficient (Chapron et al., 2000).

For the model, a corresponding mss is extrapolated from the $\mathrm{mss}_{3\mathrm{m}}$ integrated over the limited frequency range of the model which as a maximum frequency of 0.72 Hz that corresponds to a wavelength of 3 m, using the linear dispersion relation. For this we use an expression adapted from (Vandemark et al., 2004),

$$\mathrm{mss}_{\mathrm{Ku,model}} = \mathrm{mss}_{3\mathrm{m}} + 0.0035 + 0.0093\log(U_{10}), \tag{4}$$

$$\mathrm{mss}_{3\mathrm{m}} = \int_0^{2\pi}\int_0^{0.72\mathrm{Hz}} k^2 E(f,\theta)\mathrm{d}f\mathrm{d}\theta, \tag{5}$$

where U_{10} is the wind speed, $E(f,\theta)$ the directional wave spectrum and k the wave number.

The observed mean square slope follows the behavior shown in Ardhuin et al. (2010), with an increase as a function of both wind speed and wave height (not shown here for the mss, but shown for the Stokes drift in the next section). That behavior is well captured with the new TEST451 parameterization whereas it was poorly reproduced with the BJA parameterization (not shown here). The spatial distribution of the errors on the mss are shown in Fig. 5. Not surprisingly, the large mss errors, when biases are also small, are also related to areas with larger errors in significant wave heights H_s. This is the case off the US East Coast, the Mediterranean, and the Western Pacific. However, the relative errors on the mss in that region are less than the relative errors in H_s. Because the mss is strongly correlated to the wind speed, it suggests that these errors in wave height are associated with significant wave model errors, and not just wind errors.

3.4. The surface Stokes drift

In general, the Stokes drift at the surface, hereinafter U_{ss}, is the dominant source of wind-correlated drift of surface waters (e.g., Rascle and Ardhuin, 2009; Ardhuin et al., 2009), but it is also the likely source of mixing in the upper ocean via Langmuir circulations (e.g., Leibovich, 1980; Li and Garrett, 1997; Harcourt et al., 2006; Sullivan and McWilliams, 2010; Van Roekel et al., 2012). As a result, U_{ss} is an important parameter for a wide range of applications.

Compared to the mean square slope, the Stokes drift is more influenced by the longer waves, and thus more weakly correlated with the wind speed. Indeed, Ardhuin et al. (2009, Eq. (C3)) showed that U_{ss} could be accurately predicted from the wind speed and significant wave height alone, with a rather poor variability predicted with the BJA parameterizations used in part I. U_{ss} can be expressed in terms of the wave spectrum,

$$U_{ss} = \left|\int_0^{2\pi}\int_0^{0.72\mathrm{Hz}} 4\pi f k(\cos\theta,\sin\theta)E(f,\theta)\mathrm{d}f\mathrm{d}\theta\right|. \tag{6}$$

Please cite this article in press as: Rascle, N., Ardhuin, F. A global wave parameter database for geophysical applications. Part 2: Model validation with improved source term parameterization. Ocean Modell. (2013), http://dx.doi.org/10.1016/j.ocemod.2012.12.001

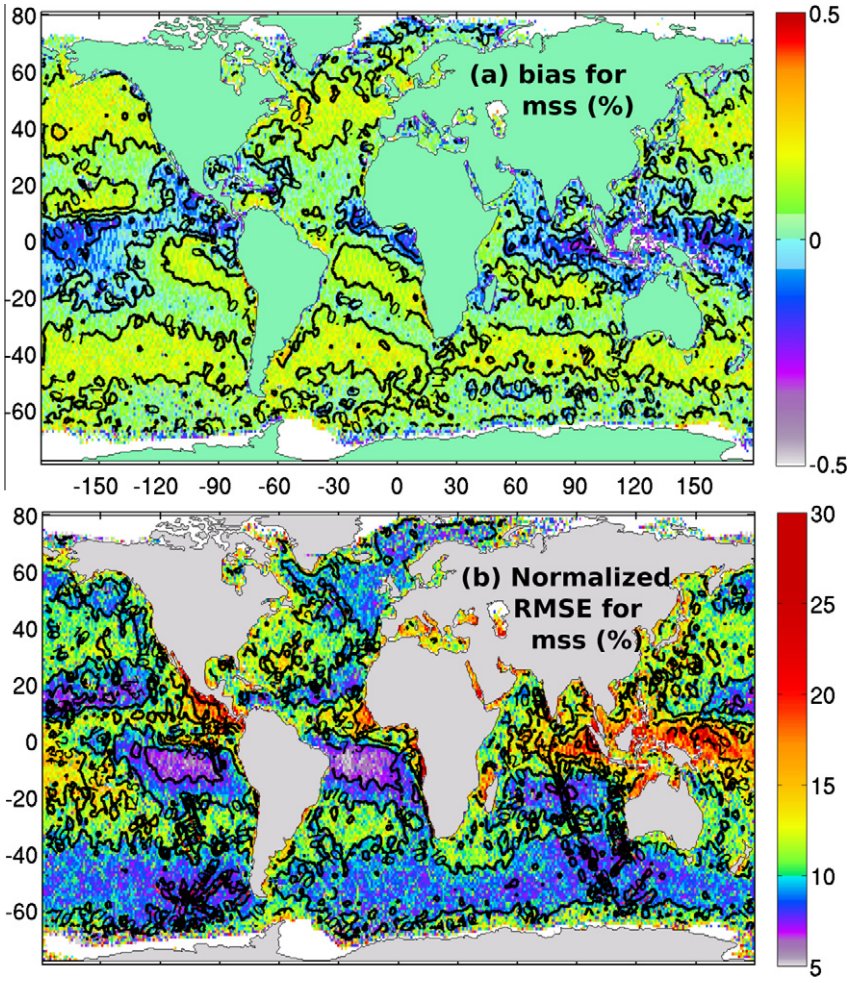

Fig. 5. (a) Bias and (b) scatter index for the modelled mean square slopes for the year 2005, against data from Jason-1, Jason-2 and Envisat altimeters. The new parameterization TEST451 is used with the CFSR wind forcing. Both model and altimeter data are averaged along the satellite tracks over 1 degree in latitude. There are 2.4 million averaged values.

Contributions to U_{ss} drift have been limited here to wave frequencies less than 0.72 Hz, which may underestimate the full spectral contribution by 0.25 to 0.5% of the wind speed (Rascle et al., 2008 their Fig. 8).

Although the Stokes drift is seldom measured directly, using drifting buoys, Eq. (6) is a very good approximation of the wave-induced drift, even when finite amplitudes are considered, with the exception of waves in shallow water (Ardhuin et al., 2008). As a result, U_{ss} can be validated using data from directional wave buoys (e.g., Ardhuin et al., 2009). In particular, for linear waves, U_{ss} can be estimated from the wave spectrum $E(f)$ and the directional spreading $\sigma_\theta(f)$,

$$U_{ss} = \int_0^{f_c} \frac{1}{g}(2\pi f)^3 E(f)(1-\sigma_\theta^2)\mathrm{d}f \tag{7}$$

with $\sigma_\theta(f)$ defined following Kuik et al. (1988), and expressed in radians. Here the integral is stopped at a cut-off frequency $f_c = 0.4$ Hz in order to allow a comparison with buoy data in the range of frequencies where they can be trusted.

The validation of the Stokes drift, including this directional effect, is extended from Ardhuin et al. (2009) to a larger range of wave climates, and summarized in Table 2. Model results with the BJA parameterizations are also shown for comparison with the results presented in Part I. We have included buoys from the Gulf of Alaska (46001), Pacific Northwest coast of the United States (46002), Hawaii (51001), Central California (46013 and 46214), in the Central Pacific (Kiribati, 51028), 400 km west of Bermuda (41048), off Nantuckett island (44008), and 10 km south-east of the French island of Ouessant (62069). Data from that latter buoy has been used in Ardhuin et al. (2009) and it is strongly affected by tidal currents. For these reasons the time step of the model and data is reduced to 1 hour and the model results are taken from the unstructured Iroise grid, which is also forced by tidal currents and water levels. In the comparison the same cut-off frequency is used for the model and buoy data.

Model biases against the buoy data are very much associated with wind biases in the case of the new TEST451 parameterization. The two buoys 46214 and 46013 are only separated by 35 km, but the wind at the buoy which is closest to shore (46013), is much more strongly underestimated, in particular in situations of along-shore wind jets. Errors are typically less with this new parameterization compared to model results with BJA. The difference is particularly striking in the Pacific, e.g., at buoys 46001 and 46002, and it is due to spurious swell-wind sea interactions caused by the BJA dissipation parameterization that reduces strongly the high frequency tail, and thus the Stokes drift, in the presence of swell. The errors reported here are also typically 30% less than the errors reported by Tamura et al. (2012), but their larger error is likely caused to a large extent by less accurate winds from an older re-analysis.

Please cite this article in press as: Rascle, N., Ardhuin, F. A global wave parameter database for geophysical applications. Part 2: Model validation with improved source term parameterization. Ocean Modell. (2013), http://dx.doi.org/10.1016/j.ocemod.2012.12.001

Table 2
Model accuracy for U_{ss} estimated by the model and from wave buoy spectra for the year 2008. The models are forced with ECMWF winds and use either the new TEST451 parameterization or the BJA parameterization. Buoys are referenced by their WMO identification code. Details on the instrument packages and locations can be found at www.ndbc.noaa.gov . The normalized bias (NB) is defined as the bias divided by the r.m.s. observed value, the scatter index (SI) is defined by Eq. (2), and r is Pearson's correlation coefficient. All buoy spectra were averaged over 3 hours (except for 1 hour at 62069) before integrating in frequency from 0.037 to 0.405 Hz and computing these statistics. Wind speeds were averaged quadratically over the same time frame after a 10% increase, which is an approximate bias correction for the 5 m anemometer height of the buoys. For directional buoys 46013, 46214, 41048, the Stokes drift includes the reduction due to the directional spreading.

	Buoy ID	TEST451 ECMWF			BJA		
		NB (%)	SI (%)	r	NB (%)	SI (%)	r
U_{10}	46001	−2.5	12.1	0.961			
H_s	46001	−1.2	13.4	0.962	−5.0	15.9	0.946
U_{ss}	46001	−8.3	14.8	0.966	−22.6	23.3	0.930
U_{10}	46002	−3.8	11.9	0.966			
H_s	46002	2.5	9.5	0.975	0.2	11.2	0.962
U_{ss}	46002	−8.4	11.5	0.979	−20.1	19.8	0.952
U_{10}	51001	−6.8	9.1	0.967			
H_s	51001	0.3	10.4	0.942	−1.0	13.1	0.907
U_{ss}	51001	−9.3	14.4	0.950	−18.9	18.3	0.933
U_{10}	46013	−19.5	23.1	0.924			
H_s	46013	−5.0	13.5	0.950	−4.0	16.1	0.936
U_{ss}	46013	−21.3	24.9	0.942	−24.0	26.6	0.938
H_s	46214	−2.4	12.1	0.957	0.4	12.8	0.956
U_{ss}	46214	2.8	16.5	0.959	0.13	17.2	0.952
U_{10}	51028	−13.6	8.5	0.895			
H_s	51028	3.0	9.1	0.898	6.4	12.2	0.789
U_{ss}	51028	−7.4	14.6	0.960	−14.5	18.8	0.928
U_{10}	42036	−8.0	18.7	0.925			
H_s	42036	−16.5	15.6	0.966	−19.6	16.2	0.965
U_{ss}	42036	−15.1	20.2	0.960	−22.3	24.1	0.956
U_{10}	41048	−10.9	1.50	0.949			
H_s	41048	−6.0	15.3	0.940	0.0	13.5	0.954
U_{ss}	44008	4.6	25.5	0.916	15.0	23.7	0.944
U_{10}	44008	1.3	18.3	0.929			
H_s	44008	−6.1	17.3	0.930	−3.4	15.9	0.943
U_{ss}	41048	−1.6	26.6	0.898	6.8	25.0	0.915
H_s	62069	7.9	10.8	0.980			
U_{ss}	62069	21.9	27.7	0.953			

Looking at the general climatology of the Stokes drift, we find a significant increase of U_{ss} with the wave development, growing from 1% of the wind speed for small wave heights, to 2% of the wind speed for large wave heights (Fig. 6a). This increase with H_s was poorly captured by the BJA parameterization which reduces the spectral tail level when the waves become more mature, resulting in lower ratios U_{ss}/U_{10} and less variations with wave development (Fig. 6b).

As a result, compared to the old parameterizations, the global yearly average of U_{ss}/U_{10} is not significantly changed over low latitudes, with values around 0.8 to 1% (Fig. 7). However, at mid and high latitudes, this ratio is strongly increased from 1.1 to

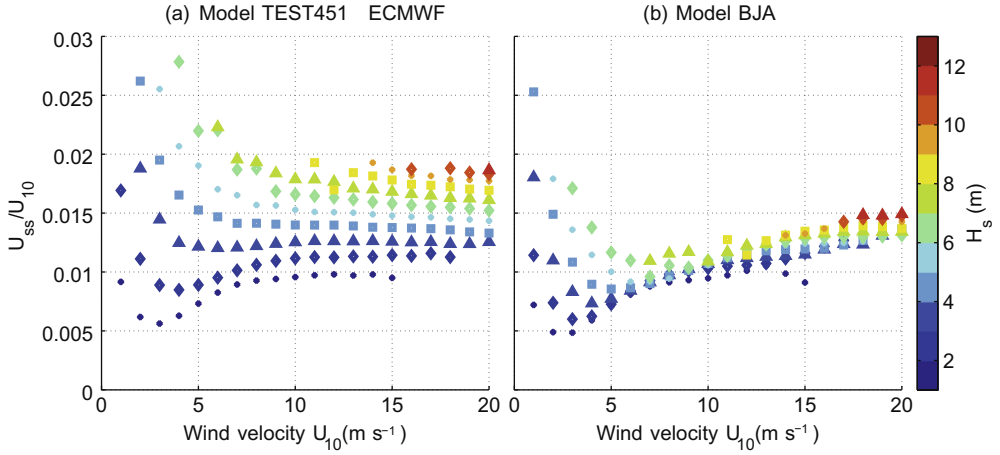

Fig. 6. Average modelled ratios U_{ss}/U_{10} from the global 0.5-degree resolution model domain. U_{ss} is estimated using Eq. (6) and cut here at 0.72 Hz. (a) Uses the new TEST451 parameterization whereas (b) uses the BJA parameterization as in part I, both forced by ECMWF winds. Averages are taken after the model output has been binned with bins of 1 m significant wave height and 1 m/s wind speed.

Please cite this article in press as: Rascle, N., Ardhuin, F. A global wave parameter database for geophysical applications. Part 2: Model validation with improved source term parameterization. Ocean Modell. (2013), http://dx.doi.org/10.1016/j.ocemod.2012.12.001

1.5%, due to larger Stokes drift for medium to strong winds in the new parameterizations.

We note that the ratio U_{ss}/U_{10} is reduced when using CFSR winds because these winds are stronger and the wave model has been adjusted to give similar results than with the lower ECMWF winds. Still, this difference is less than the difference between the two parameterizations BJA and TEST451.

4. Wave directionality and seismic noise sources

4.1. Wave directionality

The new parameterization TEST451 generally produces mean directions and directional spreadings that agree better with buoy data. This is partly due to the better representation of swell fields,

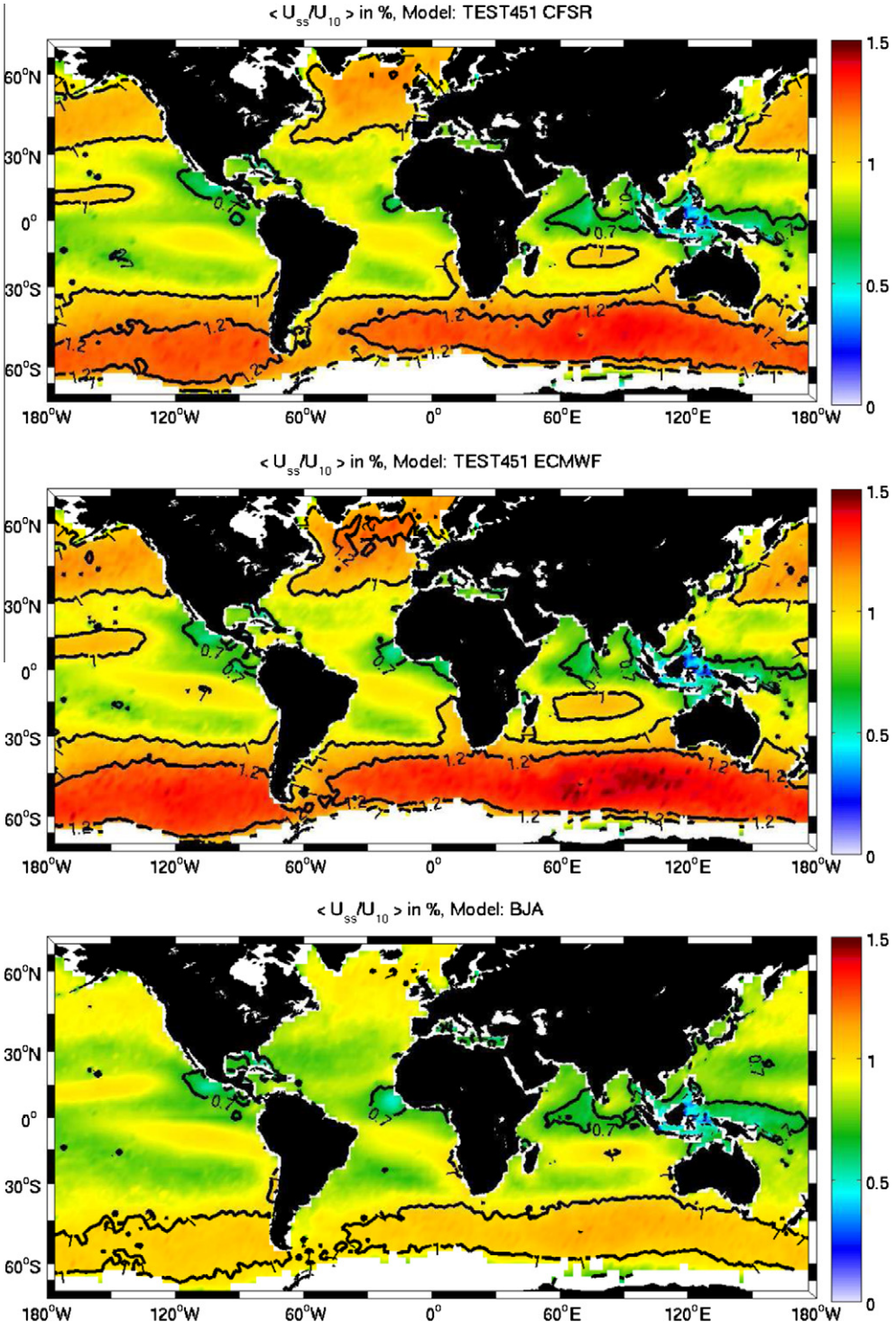

Fig. 7. Annual mean of the ratio U_{ss}/U_{10} for the year 2005, where U_{ss} is cut at 0.72 Hz. Model results are shown for the new parameterization TEST451 using CFSR winds (top panel) and using ECMWF winds (middle panel). The results with the BJA parameterization (and using ECMWF winds) are shown in the bottom panel.

Please cite this article in press as: Rascle, N., Ardhuin, F. A global wave parameter database for geophysical applications. Part 2: Model validation with improved source term parameterization. Ocean Modell. (2013), http://dx.doi.org/10.1016/j.ocemod.2012.12.001

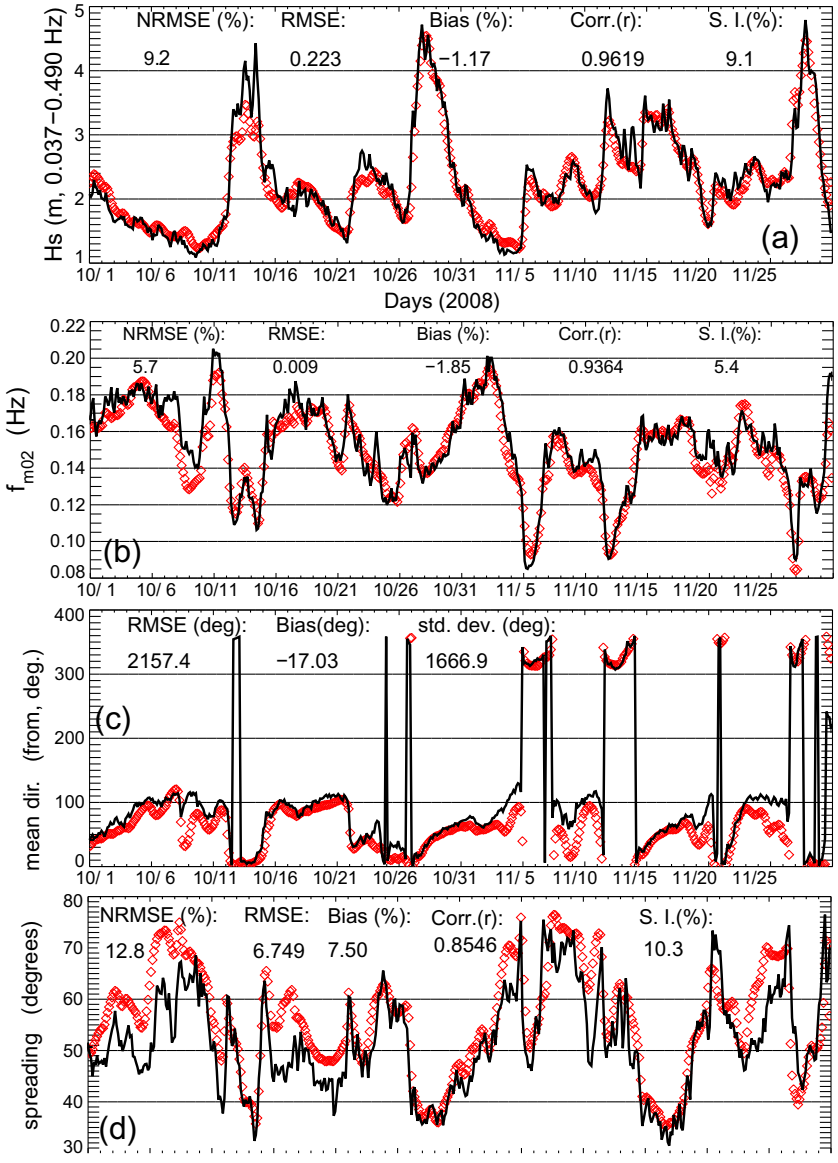

Fig. 8. Time series of observed and modelled wave height, mean frequency, mean direction and directional spread at the buoy number 51001, located to the north-west of Hawaii. The model uses the new TEST451 parameterization with the CFSR winds.

but it is also true when considering only the wind seas. For example, looking at waves in the 0.25 to 0.5 Hz at the 51001 buoy, located north-west of Hawaii, the rms error on the mean direction is reduced from 20.3 to 18.4 degrees, over the year 2008, and the directional spread estimated from the first moments has an error reduced from 15.9% to 10.1%, with a correlation increased from 0.64 to 0.77. Similar improvements are found at other locations, including enclosed seas such as the Gulf of Mexico. However, the directional spreading in coastal areas is sensitive to shoreline reflections (Ardhuin and Roland, 2012), while larger offshore buoys are expected to produce more noisy estimates of this parameter (O'Reilly et al., 1996). In the hindcast presented here, the coefficient for energy reflection at the shoreline is set to a constant value of 0.05, which fails to capture the large variability due to coastal morphology, from 0.5 in front of steep cliffs (O'Reilly et al., 1999) to less than 0.01 for beaches with very small slopes (Elgar et al., 1994).

The quality of a typical open ocean time series of wave parameters is illustrated in Fig. 8, for the buoy 51001 at the end of 2008. Wave heights in the time series are dominated by North Pacific storms with wind and wave directions from the North to East in Fig. 8b. The frequency content of the wave spectrum is generally very well reproduced with only a slight positive bias at the lowest frequencies. The mean frequency f_{m02} is, as in all other locations, very well reproduced by the present parameterization with virtually no bias and random errors below 6%. This is a typical reduction of random error by 20% compared our model result using the BJA parameterization. In terms of direction, however, there seems to be some persistent bias for Southerly swells by 20 degrees or so, that introduces a bias in the mean direction. That bias is reduced compared to runs with the BJA parameterization. For frequencies above 0.17 Hz, the bias varies from −9 to −7 degrees, and the BJA parameterization gives slightly stronger biases except at the highest frequencies. At these frequencies the bias is mostly associated to turning winds (e.g., Guillaume, 1990) and the rate of rotation of the mean wave direction in the wind sea. The time lag between the model and the measurements is associated to the strength of the source terms, just like the obliqueness of the wave direction in slanting fetch conditions (Ardhuin et al., 2007). The stronger the source terms, the smaller the time lag. Here the model

Please cite this article in press as: Rascle, N., Ardhuin, F. A global wave parameter database for geophysical applications. Part 2: Model validation with improved source term parameterization. Ocean Modell. (2013), http://dx.doi.org/10.1016/j.ocemod.2012.12.001

seems to perform rather well. We have not performed a rotary co-spectral analysis that can be used to quantify this effect (e.g., Ardhuin et al., 2009).

The directional spreads at the buoy 51001 are slightly overestimated, with a bias of the order of 7%, that corresponds to about 5 degrees. The buoy measurements are also expected to be biased high by a few degrees also (O'Reilly et al., 1996), making the true model bias possibly as high as 10%. However, this total spread comes from both the spread at each frequency and the fact that the mean directions are different at different frequencies. When each frequencies are inspected the spread bias, compared to the buoy, increases from -5% at $f = 0.08$ Hz to 2% around 0.15 Hz and decreases again to -5% for $f > 0.3$ Hz. This is not very different from results with the BJA parameterization, except for these higher frequencies where the BJA parameterization gives biases of the order of -15%, which we attribute to their use of a strong dissipation term in that range and its isotropic nature. The underestimation of directional spreading at these high frequencies is consistent with the underestimation of underwater acoustic measurements at frequencies around 1 Hz (Ardhuin et al., paper in revision for the Journal of the Acoustical Society of America).

4.2. Seismic noise sources

Recent developments in the study of seismic noise have shown that the noise spectra at seismic stations could be predicted with a good degree of confidence (Ardhuin et al., 2011b) and that, conversely, seismic noise could be used, in particular along the US West Coast, to estimate the significant wave height and mean period (Ardhuin et al., 2012). This seismic noise is very sensitive to the directional distribution of the wave energy: noise is generated at twice the frequency of the waves if and only if there are some wave trains with the same frequency that propagate in opposite directions (Longuet-Higgins, 1950). More specifically, the level of noise sources at any point of the ocean is proportional to the directional integral

$$I(f) = \int_0^{\pi} M(f,\theta) M(f,\theta+\pi) \mathrm{d}\theta, \tag{8}$$

with M the directional distribution normalized such that $E(f,\theta) = E(f) M(f,\theta)$. These noise sources can add up over large areas to give the seismic noise recorded at any location. The typical ocean area that contributes to a noise recorded at a seismic station varies from a radius of a few hundred kilometers, in the case of Central California, to several thousand kilometers in the case of Hawaii (Ardhuin et al., 2011b).

As stated above, the directional spreading and thus the seismic noise can be strongly influenced by shoreline reflections. Here we shall avoid this complication by focusing on the Kipapa seismic station (KIP) in Hawaii, for which the effect of shoreline reflection is generally negligible (Ardhuin et al., 2011b).

Academic tests performed by Ardhuin et al. (2011b) showed that different parameterizations of the wind-wave generation and dissipation could produce very different noise levels, due to the different directional distributions. In Fig. 9 the noise recorded at KIP is compared to noise modelled using the method of Ardhuin et al. (2012), based on the theories of Longuet-Higgins (1950) and Hasselmann (1963), using the two parameterizations TEST451 and BJA for the month of May 2008. Fig. 9a shows that the recorded time series of noise levels is generally well reproduced with a better rendering of all events when using the TEST451 parameterization. The other panels show the frequency spectra corresponding to these three curves and we understand better the nature of the differences. Seismic frequencies below 0.2 Hz correspond to wave frequencies below 0.1 Hz and these are dominated by swells. It is no surprise that the better swell representation with TEST451 gives results for these low frequencies that agree better with the measurements. We also note that the upgrade from TEST441b used by Ardhuin et al. (2011b) and Stutzmann et al. (2012) to TEST451 (see Appendix B) has dramatically improved the modelling of seismic noise in the central Pacific with a correlation between model and data from the seismic station of Papeete (French Polynesia) increased from 0.71 to 0.91.

More interesting is the relative higher noise level at high frequencies, which is often associated with wind seas. It appears that TEST451 gives a higher noise level than BJA, meaning that TEST451 gives more energy propagating in opposite directions, and this seems to be in a better qualitative agreement with the recorded

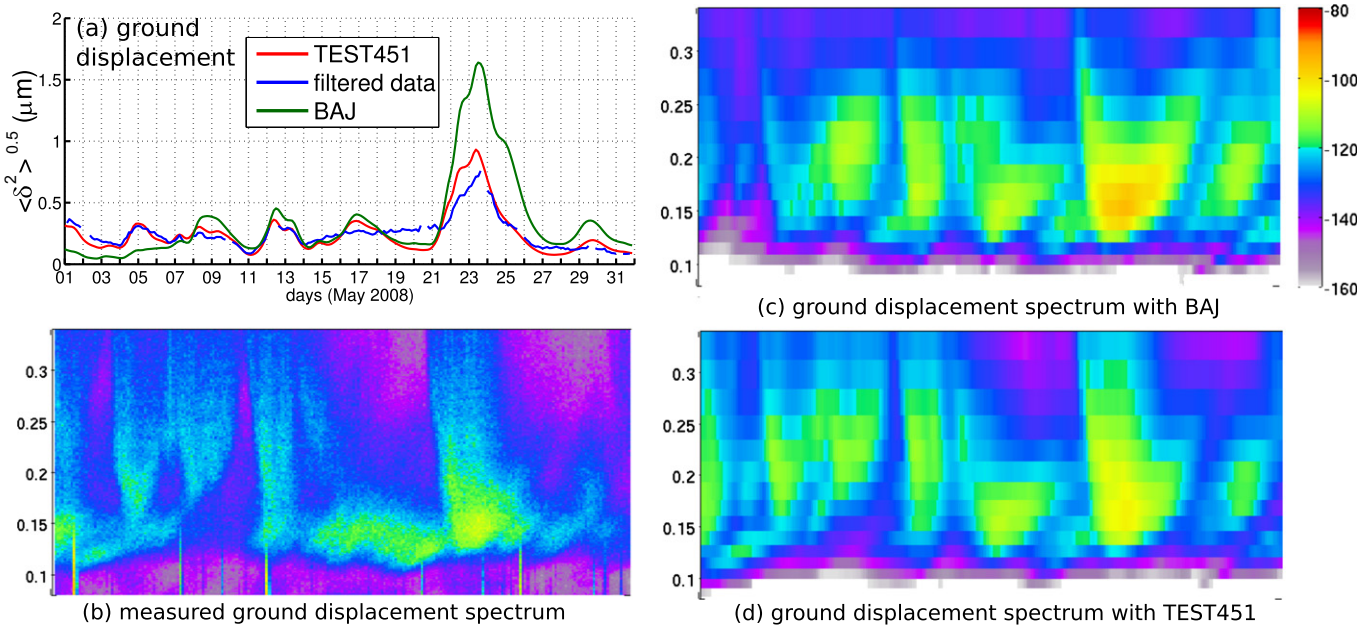

Fig. 9. (a) Time series of vertical ground motion variance recorded and modelled at the Hawaiian Kipapa station during May 2008. (b) Power spectral density of recorded vertical ground displacement at Kipapa. The colors give the spectral level in dB relative to 1 m^2/Hz. (c, d) Modelled spectra of ground displacement at Kipapa based on the numerical wave model using either the BJA or TEST451 parameterizations, both forced by ECMWF winds.

Please cite this article in press as: Rascle, N., Ardhuin, F. A global wave parameter database for geophysical applications. Part 2: Model validation with improved source term parameterization. Ocean Modell. (2013), http://dx.doi.org/10.1016/j.ocemod.2012.12.001

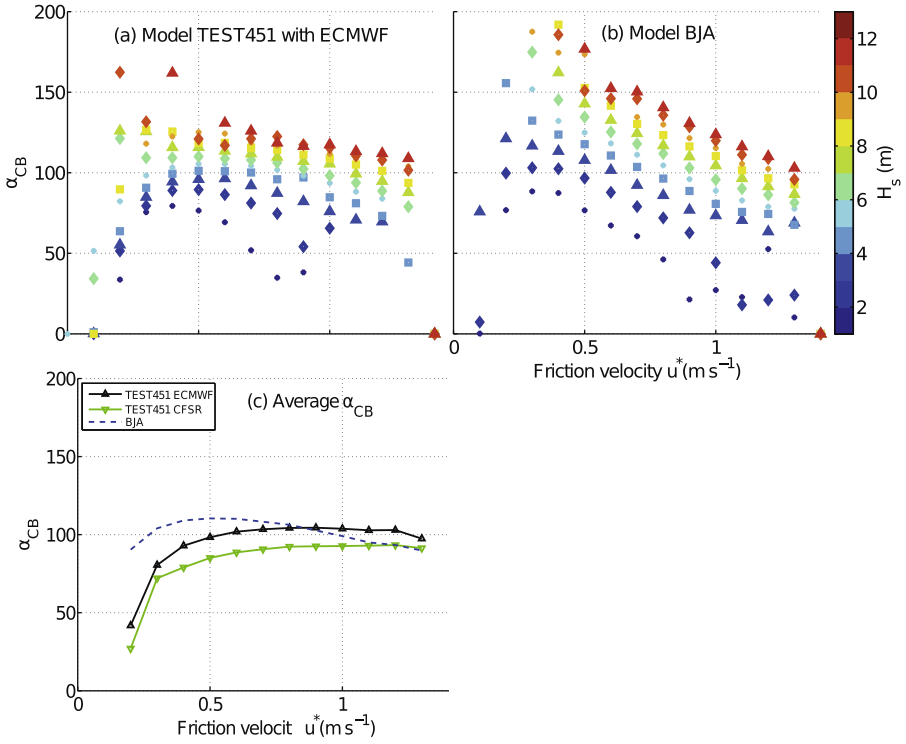

Fig. 10. Craig and Banner (1994)'s parameter α_{CB} of waves to ocean energy flux as a function of u^* and H_s. (a) For the new parameterization TEST451 with ECMWF. (b) For the parameterization BJA. (c) As a function of u^* only, and for the different models and wind forcings.

noise, than the result of the model with the BJA parameterization. This is consistent with our analysis of modelled directional spreads.

5. Air–sea fluxes of energy and momentum

5.1. Production of turbulence by wave breaking

Most of the wind energy input to surface waves is dissipated by wave breaking, which likely represents the dominant source of turbulent kinetic energy (TKE) in the first few meters below the surface (Terray et al., 1996; Gemmrich et al., 2008). Direct measurements of the energy flux from waves to ocean Φ_{oc} are difficult, thus diagnostics from a realistic wave model might help to estimate that flux, especially at global scale. Since the new parameterization TEST451 improves both low (e.g., H_s) and high (mss, U_{ss}) order spectral moments, there is a fair chance that the representation of the fluxes in and out of the wave field are also improved.

The energy flux (in W m^{-2}) is generally parameterized with the non-dimensional Craig and Banner (1994)'s parameter α_{CB}, defined by

$$\Phi_{oc} = \frac{\rho_a^{3/2}}{\rho_w^{1/2}} \alpha_{CB} u^{*3}, \tag{9}$$

where $u^\star$ is the air side friction velocity and ρ_a and ρ_w are the air and water densities. α_{CB} depends on the wave age (e.g., Terray et al., 1996), but because the peak wave speed C_p is a fairly noisy quantity when estimated from real sea states that contain swell, we prefer to use the significant wave height as a surrogate for the wave age.

The new parameterization displays the same sensitivity of α_{CB} to the wave development as the BJA parameterization, with a similar spread between the energy dissipation of young and mature seas (Fig. 10a and b). However its magnitude at low/medium winds is reduced in TEST451 compared to BJA, while it is increased at large winds (Fig. 10c). Adjustment of the wind-wave growth parameter $\beta_{\max}$ of the new parameterization TEST451 to accommodate to the different wind forcings can be directly traced to the α_{CB} parameter, which is 15% larger in the CFSR compared to the ECMWF version (Fig. 10c).

The energy fluxes from atmosphere to waves Φ_{aw} and from waves to ocean Φ_{oc} overall depend on the wind speed, on the drag coefficient and on the α_{CB} parameter. As shown in Table 3, the fluxes are reduced by 20% in the new parameterization, with yearly averages around $\Phi_{aw} = 56$ TW and $\Phi_{oc} = 52$ TW, to be compared to 72 and 68 TW using BJA, which is very close to the numbers given in Part 1, and comparable to the estimates of Wang and Huang (2004). Those energy fluxes are mostly concentrated in the winter storms, with a dominance of the Southern Ocean (Fig. 11).

5.2. Production of turbulence by the Stokes drift shear

Another interesting flux of energy is the flux from wave energy to the upper ocean TKE associated with the stretching of turbulence by the Stokes drift (e.g., Ardhuin and Jenkins, 2006). This particular flux is expected to be the source of the Langmuir turbulence

Table 3
Average over the year 2005 of the global fluxes of energy from atmosphere to waves Φ_{aw} and from waves to ocean Φ_{oc}, for the BJA parameterization and for the new TEST451 parameterizations with ECMWF and CFSR winds.

Model forcing	BJA ECMWF	TEST451 ECMWF	TEST451 CFSR
$\rho_a^{1.5}\rho_w^{-0.5}u^{*3}$ (TW)	0.68	0.61	0.67
Φ_{oc} (TW)	68	53	51
Φ_{aw} (TW)	72	57	55

Please cite this article in press as: Rascle, N., Ardhuin, F. A global wave parameter database for geophysical applications. Part 2: Model validation with improved source term parameterization. Ocean Modell. (2013), http://dx.doi.org/10.1016/j.ocemod.2012.12.001

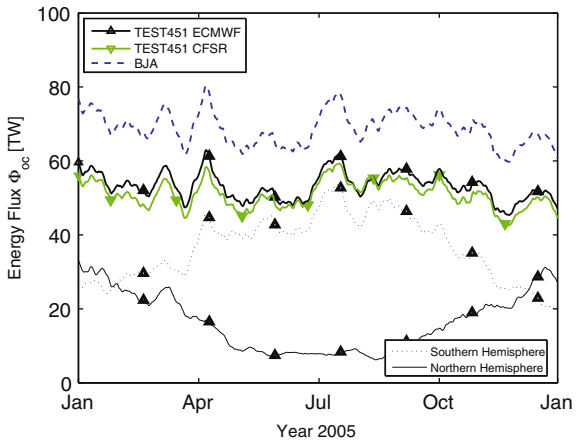

Fig. 11. Global fluxes of energy Φ_{oc} from waves to ocean in 2005, for the three datasets BJA, TEST451 ECMWF and TEST451 CFSR. The BJA parameterization is 20% larger. For TEST451 ECMWF, the distribution between Northern and Southern Hemisphere is shown. All time series have been low-pass filtered at 30 days.

which has a strong impact on the mixed layer dynamics (Kantha and Clayson, 2004; Noh et al., 2009; Sullivan and McWilliams, 2010). This term was neglected as a dissipation term in TEST451 because it is typically one order of magnitude less than the wave breaking dissipation, we shall estimate it here diagnostically.

As discussed by Kantha (2006), this Stokes-shear energy flux writes

$$\Phi_{St} = -\int_{-\infty}^{0} \vec{\tau}.\frac{\partial \vec{U}_s}{\partial z}\mathrm{d}z, \qquad (10)$$

where $\vec{\tau}$ is the shear (Reynolds) turbulent stress and $\vec{U}_s$ is the Stokes drift. Φ_{St} can be written as a fraction of the work of the wind stress on the surface Stokes drift, $\Phi_{St} = \alpha_K \vec{\tau}_w.\vec{U}_{ss}$, with the coefficient α_K depending on the profile of the Stokes drift, on the stratification, on the Earth rotation and on turbulence intensity within the ocean. The product $\vec{\tau}_w.\vec{U}_{ss}$ gives a global energy flux of 7 TW. Note that the explicitly resolved waves (up to 0.72 Hz) account for 5.5 TW, the remaining part being calculated using a parametric high frequency tail. This is consistently larger than our previous estimate of 6 TW (Rascle et al., 2008), since the Stokes drift was underestimated with the BJA parameterization (see Section 3.4).

Kantha (2006) estimated α_K for different monochromatic waves, and Kantha et al. (2009) retained an average value of 0.65. Using this value of α_K, we find that $\Phi_{St} = 4.5$ TW are available to fuel to Langmuir circulations. This estimation is much larger than the 2.5 TW of Kantha et al. (2009), presumably because their wave spectra are truncated at a maximum frequency of 0.4 Hz and thus underestimate the Stokes drift (Rascle et al., 2008).

Similarly to the total wave dissipation, this production of turbulence by the Stokes drift is largely seasonal because it is concentrated in the winter storms (not shown, similar in trend to Fig. 11).

5.3. Momentum fluxes

With the better reproduction of the mss and U_{ss} that are strongly dependent on the spectrum high frequency tail, we expected that the wave-supported stress and wind drag coefficient should also be better reproduced by the new parameterization TEST451. Indeed, for a wind input proportional to the $1/C^2$, with C the phase speed, the wave-supported stress is directly proportional to the upwind-downwind mean square slope (e.g., Plant, 1982; Juszko et al., 1995).

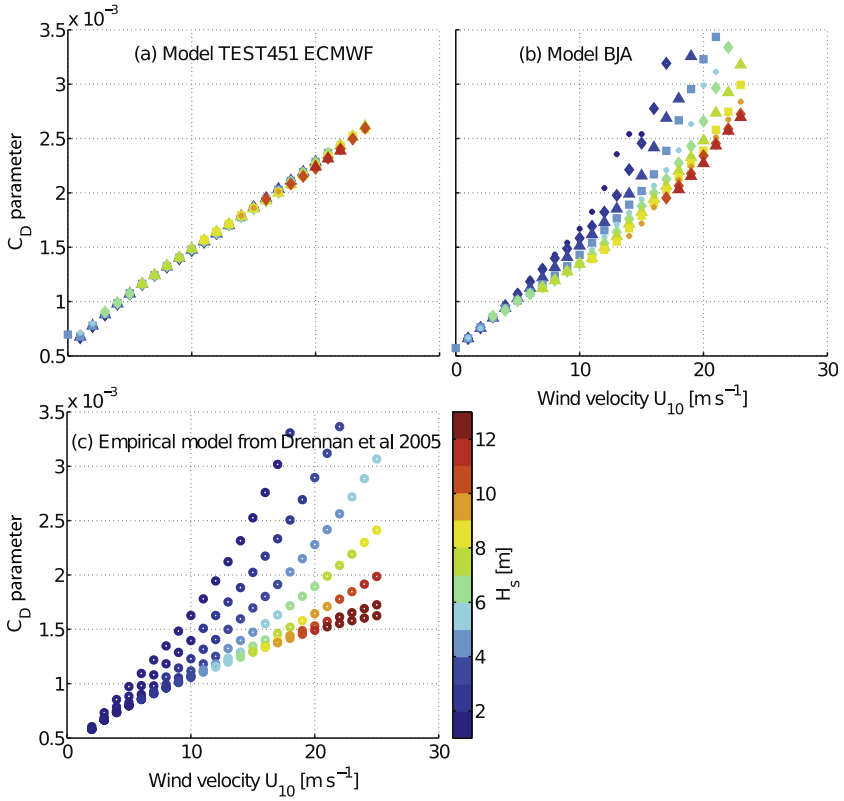

Fig. 12. (a) Drag coefficient C_D for the new parameterization TEST451 with ECMWF winds. (b) For the BJA parameterization used in Part I. (c) Expected with the empirical formulation of Drennan et al. (2005) their Eq. (4). For the latter, the C_D is a function of H_s and the wave age, thus we suppose pure wind-sea conditions and we vary the wind and the fetch, with the wind-wave growth taken from Elfouhaily (1997).

Please cite this article in press as: Rascle, N., Ardhuin, F. A global wave parameter database for geophysical applications. Part 2: Model validation with improved source term parameterization. Ocean Modell. (2013), http://dx.doi.org/10.1016/j.ocemod.2012.12.001

Table A.4
Gridded parameters archived in the database. WBBL means wave bottom boundary layer.

Subfolder	Contents	Practical remarks
hs	H_s	Units are meters, do not forget the scale factor
t	$T_{m0,-1}$	Mean period corresponding to -1 moment
t02	$T_{m0,2}$	Mean period corresponding to 2nd moment
CgE	Energy flux	In watts per meter, useful for marine energies
dir	θ_{mean}	Mean direction of the full spectrum
dp	θ_p	Mean direction at the peak frequency
spr	σ_θ	Directional spreading of the full spectrum
partitions	$H_{s,i}, T_{p,i}, \theta_{s,i}$	Significant height, period and direction of swell partition number i, with i from 0 to 5. 0 is windsea, 1 to 5 are swells
wsf	Wind sea fraction	Fraction of wave energy in the wind sea partition
hsw	'Wind sea' height	Wave height of components with a positive wind input
ice	Sea ice	Sea ice concentration: this is a forcing field
wnd	U_{10}	Wind vector components: this is a forcing field (n.a. for ECMWF)
cur	Current	Current vector components: this is a forcing field
dpt	Water depth	Bathymetry plus water level: this is a forcing field
abr	a_b	r.m.s. amplitude of water particle displacement at top of WBBL Warning: the significant value is $\sqrt{2}a_b$
ubr	u_b	r.m.s. amplitude of wave-induced velocity at top of WBBL. Warning: the significant value is $\sqrt{2}u_b$
mss	$(\mathrm{mss}_x, \mathrm{mss}_y)$	The two components of the mean square slope. mss = mss_x + mss_y
ust	$u_\star$	Friction velocity in the air, $\tau = \rho_a u_\star^2$
faw	Φ_{aw}	Wind to waves energy flux in W/m^2
foc	Φ_{oc}	Waves to ocean energy flux in W/m^2
taw	τ_{aw}/ρ_w	Wind to waves momentum flux
two	τ_{oc}/ρ_w	Waves to ocean momentum flux
uss	U_{ss}	Surface Stokes drift vector (with a frequency cut-off at 0.72 Hz)
tus	T_s	Stokes drift transport vector
wcc	Whitecap coverage	Fraction of sea surface covered by active whitecaps
wcf	Foam thickness	Average thickness of all foam produced by whitecaps

We shall thus examine the variability of the drag coefficient, expressed as

$$C_D = \frac{u^{\star 2}}{U_{10}^2}. \tag{11}$$

This drag coefficient is known to increase with the wind speed, but it is also believed to depend on the wave age, with larger values for steep young waves (see Drennan et al. (2005) for a review of dedicated field experiments). Other experiments do not necessarily report such a strong dependence (Edson et al., 2007), but that can be due to inherent correlation of wind speed with wave age in such datasets. A quantitative calculation is shown in Fig. 12c, where we use the empirical formulation of Drennan et al. (2005, their Eq. (4)), which is written

$$C_D = \left(\frac{1}{\kappa}\log\frac{10}{z_0}\right)^{-2}, \quad \text{with} \quad \frac{z_0}{H_s} = 3.35\left(\frac{u^\star}{C_p}\right)^{3.4}. \tag{12}$$

In comparison, the BJA parameterization yields a reasonable dependence of C_D (Fig. 12b), while the new parameterization TEST451 appears all but independent on the wave age (Fig. 12a). This is clearly due to the only change in the wind input parameterization, namely the introduction of a sheltering effect which reduces the apparent stress for the shorter wave components. Further work is clearly needed to improve and validate the air-waves-sea momentum exchange in the new parameterization, in particular as the wave-supported stress might be unrealistic. Further work will likely investigate how the sheltering term can be reduced. That will probably require an increase in the dissipation to keep the correct balance in the spectral tail. Since the friction velocity $u^\star$ is not just a diagnostic parameter of the wave model but a parameter that comes into the wind-generation term, it is also expected that increasing $u^\star$ specifically for young waves may help reduce the low wave height bias at short fetch.

6. Conclusion

A 20 year hindcast of global wave parameters has been produced using a new parameterization for wave dissipation (Ardhuin et al., 2010), and forcing from a combination of ECMWF analysis and CFSR reanalyses, sea ice from CFSR and ECMWF and icebergs from CERSAT.

The continuous validation with altimeter and buoy data reveals several important facts related to wind forcing,

- CFSR winds are anomalously high in the Southern Ocean for the years 1991–1993, compared to following years, resulting in anomalous high biases for these years, including off the U.S. West coast. This bias is corrected for the following years, probably due to the start of SSM-I data assimilation in CFSR. This and other patterns in CFSR winds have been discussed by Cox et al. (2011) and Chawla et al. (2012).
- CFSR and NCEP analyses have systematically higher values than ECMWF analyses of the wind speed, and this is even more true for the highest speed range.
- A simple calibration of the wind wave growth parameter, $\beta_{\max} = 1.33$ for CFSR or NCEP winds compared to $\beta_{\max} = 1.52$ for ECMWF winds corrected the average to high wave heights.
- Modelled wave heights are still too low for the highest values ($H_s > 12$ m), likely due to an underestimation of the winds in these conditions, as shown for a specific storm by Hanafin et al. (2012).

Besides those considerations of wind forcing, the new parameterization provides significantly improved hindcasts compared to those of Part 1 (Rascle et al., 2008),

- The dominant wave parameters (wave height, peak period) are improved, especially in swell-dominated regions like the Central Pacific.
- The improvement is particularly large for the mean square slope of the sea surface, which is now relatively well estimated with the model and may be a useful parameter for remote sensing applications.
- Following the mss improvements, the new parameterization improves the estimations of the surface Stokes drift, as validated with buoy data. The Stokes drift is thus in global average larger than previously estimated, and so is the energy available for near-surface Langmuir turbulence.
- We have explored the directionality of the wave field which appears generally well represented, including the directional integral $I(f)$ that appears in the source of seismic noise. Noise measurement suggests that wave spectra are fairly broad on average at frequencies above the wind-sea peak, in a way consistent with our new model results.
- The energy released by the waves through wave breaking is more difficult to validate but it is nonetheless estimated with the new model and appears significantly reduced compared to

Please cite this article in press as: Rascle, N., Ardhuin, F. A global wave parameter database for geophysical applications. Part 2: Model validation with improved source term parameterization. Ocean Modell. (2013), http://dx.doi.org/10.1016/j.ocemod.2012.12.001

previous estimations. In spite of the good behavior of the mss and of the Stokes drift, the air–sea momentum flux corresponds to a drag coefficient that varies little if at all with the wave age. The wave-supported stress and its dependency on the high frequency part thus need further development.

The hindcast database is freely available and while there are still issues and uncertainties, it might provide improved parameters for geophysical applications, including for atmospheric and oceanic modelling when used with the consistent wind reanalysis.

Acknowledgments

We thank all the providers of wind and wave measurements at NDBC, CDIP, SHOM, CNES, NASA, ESA, and ISA that have been critical for assessing the quality of wind and wave models. Seismic data was taken from the GEOSCOPE data centers. We thank J.-F. Piolle and M. Accensi for their homogenization of the buoy data formats and work on NetCDF post-processing, and the entire WAVEWATCH III$^{(R)}$development team, in particular H. L. Tolman, J. H. G. M. Alves, and A. Chawla. This work is supported by a FP7-ERC young investigator grant number 240009 for the IOWAGA project, the U.S. National Ocean Partnership Program, under grant U.S. Office of Naval Research grant N00014-10-1-0383. Additional support from ESA and CNES for the Globwave project is gratefully acknowledged. N.R. also acknowledges the financial support of the ANR through the REDHOTS project.

Appendix A. Database variables, formats and organization

The database is availaible at http://tinyurl.com/iowagaftp/HINDCAST . It is organized by model domain, i.e., 'GLOBAL' for the 0.5 degree resolution grid, ATNW for the US East Coast and Gulf of Mexico, PACE for the East Pacific, ATNE for the European coasts, CRB for the Carribean, NC for New Caledonia and Vanuatu. These are the six grids of the multigrid sytem which were run simultaneously using 2-way nesting. On top of these, the unstructured grids IROISE, NORGASUG and MENORUG were run a posteriori from full spectral boundary conditions. In each model domain, files are ordered by year, and in each year by output variable with monthly files and separate files for each variable. The subfolders for all these variables are listed in Table A.4.

For each year, two types of variables have been computed and stored. The first are spectra at preselected locations (buoys and other places of interest). These spectra are contained in files named after the WMO buoy number, or the geographical position. The spectra were further processed to integrated bulk parameters such as the wave height H_s and several mean periods.

The second type of output are gridded variables that vary in horizontal space. For convenience we have used NetCDF4, in which the gridded data is stored with 2-byte integers using a scale factor. As a result, for variables that have a large dynamic range, the relative accuracy is not very good for the low values. This is the case for the energy fluxes. The scale factor has been chosen to avoid saturation. However, it is possible that there is some overflow, leading to negative energy values for example, if the variable goes over its expected maximum. We have obviously tried to avoid this situation. In the case of seismic noise source spectra, which have a huge dynamic range, the values stored are a logarithm of the actual power spectral density of pressure.

The output time step was set at 3 hours, except for the unstructured grids that are forced by tides, in which case we use a smaller 1 hour step. In order to allow a seamless combination of the different grids, the NetCDF files also contain a MAPSTA variable that corresponds to the unambiguous 'status map' `MAPSTA(IY,IX) + 8*MAPST2(IY,IX)` of the WWATCH model. When this variable is set to 8 it means that these points were excluded from the computation and the map can be filled it using the global model domain data. We have not filled in these excluded points in order to minimize the size of the files.

For further information and updates, the README file at the root of the database should be consulted.

Appendix B. Improvements of swell dissipation in parameterization TEST451

The parameterization TEST451 used in this paper is similar to the parameterization TEST441b described in Ardhuin et al. (2010), but includes a slight modification to improve swell dissipation. The essence of the modification is a smoothing of the swell dissipation function around the threshold for transition between laminar and turbulent conditions. This was done by introducing a weighted average of the laminar $S_{\mathrm{out,l}}(f,\theta)$ and turbulent $S_{\mathrm{out,t}}(f,\theta)$ dissipation source terms given by Eqs. (8) and (9) of Ardhuin et al. (2010) into a single one,

$$S_{\mathrm{out}}(f,\theta) = (0.5+\alpha)S_{\mathrm{out,l}}(f,\theta) + (0.5-\alpha)S_{\mathrm{out,t}}(f,\theta) \tag{B.1}$$

where the smoothing parameter is defined by,

$$\alpha = 0.5\tanh\left[(\pi H_s^3/(4\nu T_{\mathrm{m0,2}}) - s_4)/s_7\right] \tag{B.2}$$

where $\nu = 1.4\times10^{-5}$ m^2 s^{-1} is the air viscosity, $T_{\mathrm{m0,2}}$ is the mean wave period and $s_4 = 10^5$ m and $s_7 = 2.3\times10^5$ m are fitting parameters.

That smoothing of the swell dissipation threshold provides significant reduction in random errors in swell dominated areas such as the central Pacific (see e.g., Fig. 4b).

References

Ardhuin, F., Jenkins, A.D., 2006. On the interaction of surface waves and upper ocean turbulence. J. Phys. Oceanogr. 36 (3), 551–557.
Ardhuin, F., Roland, A., 2012. Coastal wave reflection, directional spreading, and seismo-acoustic noise sources. J. Geophys. Res. 117, C00J20.
Ardhuin, F., Herbers, T.H.C., Watts, K.P., van Vledder, G.P., Jensen, R., Graber, H., 2007. Swell and slanting fetch effects on wind wave growth. J. Phys. Oceanogr. 37 (4), 908–931.
Ardhuin, F., Rascle, N., Belibassakis, K.A., 2008. Explicit wave-averaged primitive equations using a generalized Lagrangian mean. Ocean Modelling 20, 35–60.
Ardhuin, F., Marié, L., Rascle, N., Forget, P., Roland, A., 2009. Observation and estimation of Lagrangian, Stokes and Eulerian currents induced by wind and waves at the sea surface. J. Phys. Oceanogr. 39 (11), 2820–2838.
Ardhuin, F., Rogers, E., Babanin, A., Filipot, J.-F., Magne, R., Roland, A., van der Westhuysen, A., Queffeulou, P., Lefevre, J.-M., Aouf, L., Collard, F., 2010. Semi-empirical dissipation source functions for wind-wave models: part I, definition, calibration and validation. J. Phys. Oceanogr. 40 (9), 1917–1941.
Ardhuin, F., Hanafin, J., Quilfen, Y., Chapron, B., Queffeulou, P., Obrebski, M., Sienkiewicz, J., Vandemark, D., 2011a. calibration of the IOWAGA global wave hindcast (1991–2011) using ECMWF and CFSR winds. In: Proceedings, 12th International Workshop of Wave Hindcasting and Forecasting, Hawaii.
Ardhuin, F., Stutzmann, E., Schimmel, M., Mangeney, A., 2011b. Ocean wave sources of seismic noise. J. Geophys. Res. 116, C09004.
Ardhuin, F., Tournadre, J., Queffelou, P., Girard-Ardhuin, F., 2011c. Observation and parameterization of small icebergs: drifting breakwaters in the southern ocean. Ocean Modell. 39, 405–410.
Ardhuin, F., Balanche, A., Stutzmann, E., Obrebski, M., 2012. From seismic noise to ocean wave parameters: general methods and validation. J. Geophys. Res. 117, C05002.
Ardhuin, F., Dumas, F., Bennis, A.-C., Roland, A., Sentchev, A., Forget, P., Wolf, J., Girard, F., Osuna, P., Benoit, M., 2012. Numerical wavemodeling in conditions with strong currents: dissipation, refraction and relative wind. J. Phys. Oceanogr. 42, 2101–2120.
Babanin, A.V., Young, I.R., 2005. Two-phase behaviour of the spectral dissipation of wind waves. In: Proceedings of the 5th International Symposium Ocean Wave Measurement and Analysis, Madrid, June 2005. ASCE, paper number 51.
Banner, M.L., Morison, R.P., 2010. Refined source terms in wind wave models with explicit wave breaking prediction. Part I: Model framework and validation against field data. Ocean Modell. 33, 177–189.
Banner, M.L., Young, I.R., 1994. Modeling spectral dissipation in the evolution of wind waves. Part I: Assessment of existing model performance. J. Phys. Oceanogr. 24 (7), 1550–1570.

Please cite this article in press as: Rascle, N., Ardhuin, F. A global wave parameter database for geophysical applications. Part 2: Model validation with improved source term parameterization. Ocean Modell. (2013), http://dx.doi.org/10.1016/j.ocemod.2012.12.001

Banner, M.L., Babanin, A.V., Young, I.R., 2000. Breaking probability for dominant waves on the sea surface. J. Phys. Oceanogr. 30, 3145–3160.
Bidlot, J., Janssen, P., Abdalla, S., 2005. A revised formulation for ocean wave dissipation in CY25R1. Tech. Rep. Memorandum R60.9/JB/0516, Research Department, ECMWF, Reading, UK.
Caires, S., Sterl, A., Bidlot, J.-R., Graham, N., Swail, V., 2004. Intercomparison of different wind-wave reanalyses. J. Clim. 17, 1893–1913.
Chapron, B., Kerbaol, V., Vandemark, D., Elfouhaily, T., 2000. Importance of peakedness in sea surface slope measurements. J. Geophys. Res. 105 (C7), 17195–17202.
Chawla, A., Spindler, D.M., Tolmana, H.L., 2012. Validation of a thirty year wave hindcast using the climate forecast system reanalysis winds. Ocean Modell. http://dx.doi.org/10.1016/j.ocemod.2012.07.005.
Chen, G., Belcher, S.E., 2000. Effects of long waves on wind-generated waves. J. Phys. Oceanogr. 30, 2246–2256.
Cox, A.T., Cardone, V.J., Swail, V.R., 2011. On the use of the climate forecast system reanalysis wind forcing in ocean response modeling. In: Proceedings, 12th International Workshop of Wave Hindcasting and Forecasting, Hawaii.
Craig, P.D., Banner, M.L., 1994. Modeling wave-enhanced turbulence in the ocean surface layer. J. Phys. Oceanogr. 24, 2546–2559.
Drennan, W.M., Taylor, P.K., Yelland, M.J., 2005. Parameterizing the sea surface roughness. J. Phys. Oceanogr. 35, 835–848.
Edson, J., Crawford, T., Crescenti, J., Farrar, T., Frew, N., Gerbi, G., Helmis, C., Hristov, T., Khelif, D., Jessup, A., Jonsson, H., Li, M., Mahrt, L., Mcgillis, W., Plueddemann, A., Shen, L., Skyllingstad, E., Stanton, T., Sullivan, P., Sun, J., Trowbridge, J., Vickers, D., Wang, S., Wang, Q., Weller, R., Wilkin, J., III, A.J.W., Yue, D.K.P., , Zappa, C., 2007. The coupled boundary layers and air–sea transfer experiment in low winds. Bull. Amer. Meterol. Soc. 88 (3), 341–356.
Elfouhaily, T.M., 1997. A consistent wind and wave model and its application to microwave remote sensing of the ocean surface. Ph.D. thesis, Denis Diderot University, Paris.
Elgar, S., Herbers, T.H.C., Guza, R.T., 1994. Reflection of ocean surface gravity waves from a natural beach. J. Phys. Oceanogr. 24 (7), 1503–1511.
Fichaut, B., Suanez, S., 2011. Quarrying, transport and deposition of cliff-top storm deposits during extreme events: Banneg island. Marine Geol. 283, 36–55.
Filipot, J.-F., Ardhuin, F., 2012. A unified spectral parameterization for wave breaking: from the deep ocean to the surf zone. J. Geophys. Res. 117, C00J08.
Gemmrich, J.R., Banner, M.L., Garrett, C., 2008. Spectrally resolved energy dissipation rate and momentum flux of breaking waves. J. Phys. Oceanogr. 38, 1296–1312.
Gommenginger, C.P., Srokosz, M.A., Challenor, P.G., Cotton, P.D., 2003. Measuring ocean wave period with satellite altimeters: A simple empirical model. Geophys. Res. Lett. 30 (22), 2150.
Guillaume, A., 1990. Statistical tests for the comparison of surface gravity wave spectra with application to model validation. J. Atmos. Ocean Technol. 7, 551–567.
Hanafin, J., Quilfen, Y., Ardhuin, F., Vandemark, D., Chapron, B., Feng, H., Sienkiewicz, J., Queffeulou, P., Obrebski, M., Chapron, B., Reul, N., Collard, F., Cormand, D., de Azevedo, E.B., Vandemark, D., Stutzmann, E., 2012. Phenomenal sea states and swell radiation: a comprehensive analysis of the 12–16 February 2011 North Atlantic storms. Bull. Amer. Meterol. Soc. 93, 1825–1832.
Harcourt, R.R., D'Asaro, E.A., Dec. 2006. Large Eddy Simulation of Langmuir Turbulence in Pure Wind Seas. AGU Fall Meeting Abstracts, A562+.
Hasselmann, K., 1963. A statistical analysis of the generation of microseisms. Rev. Geophys. 1 (2), 177–210.
Hasselmann, S., Hasselmann, K., Allender, J., Barnett, T., 1985. Computation and parameterizations of the nonlinear energy transfer in a gravity-wave spectrum. Part II: Parameterizations of the nonlinear energy transfer for application in wave models. J. Phys. Oceanogr. 15, 1378–1391.
Il-Ju Moon, T.H., Ginis, I., Belcher, S.E., Tolman, H.L., 2004. Effect of surface waves on air–sea momentum exchange. Part I: Effect of mature and growing seas. J. Atmos. Sci. 61 (19), 2321–2333.
Janssen, P.A.E.M., 1991. Quasi-linear theory of wind wave generation applied to wave forecasting. J. Phys. Oceanogr. 21, 1631–1642, see comments by D. Chalikov, J. Phys. Oceanogr. 1993, vol. 23 pp. 1597–1600.
Juszko, B.-A., Marsden, R.F., Waddell, S.R., 1995. Wind stress from wave slpes using Phillips equilibrium theory. J. Phys. Oceanogr. 25, 185–203.
Kantha, L., 2006. A note on the decay rate of swell. Ocean Modell. 11, 167–173.
Kantha, L.H., Clayson, C.A., 2004. On the effect of surface gravity waves on mixing in the oceanic mixed layer. Ocean Modell. 6, 101–124.
Kantha, L., Wittmann, P., Sclavo, M., Carniel, S., 2009. A preliminary estimate of the stokes dissipation of wave energy in the global ocean. Geophys. Res. Lett. 36 (2), L02605.
Kuik, A.J., van Vledder, G.P., Holthuijsen, L.H., 1988. A method for the routine analysis of pitch-and-roll buoy wave data. J. Phys. Oceanogr. 18, 1020–1034.
Leckler, F., Ardhuin, F., Reul, N., Chapron, B., Filipot, J.-F., 2011. estimation of breaking crest density and whitecap coverage from a numerical wave model. In: Proceedings, 12th International Workshop of Wave Hindcasting and Forecasting, Hawaii.
Leibovich, S., 1980. On wave–current interaction theory of Langmuir circulations. J. Fluid Mech. 99, 715–724.
Li, M., Garrett, C., 1997. Mixed layer deepening due to Langmuir circulation. J. Phys. Oceanogr. 27, 121–132.
Longuet-Higgins, M.S., 1950. A theory of the origin of microseisms. Phil. Trans. Roy. Soc. Lond. A 243, 1–35.
Noh, Y., Goh, G., Raasch, S., Gryschka, M., 2009. Formation of a diurnal thermocline in the ocean mixed layer simulated by les. J. Phys. Oceanogr. 39 (5), 1244–1257.
O'Reilly, W.C., Herbers, T.H.C., Seymour, R.J., Guza, R.T., 1996. A comparison of directional buoy and fixed platform measurements of Pacific swell. J. Atmos. Ocean Technol. 13, 231–238.
O'Reilly, W.C., Guza, R.T., Seymour, R.J., 1999. Wave prediction in the Santa Barbara channel. In: Beal, R. (Ed.), 5th California Islands Symposium, March 29–31. Mineral Management Service, Santa Barbara CA, see also report at http://www.coastalresearchcenter.ucsb.edu/cmi/files/2001-055.pdf
Phillips, O.M., 1984. On the response of short ocean wave components at a fixed wave number to ocean current variations. J. Phys. Oceanogr. 14, 1425–1433.
Plant, W.J., 1982. A relationship between wind stress and wave slope. J. Geophys. Res. 87, 1961–1967.
Queffeulou, P., Croizé-Fillon, D., 2010. Global altimeter SWH data set, version 7, May 2010. Tech. rep., Ifremer.
Rascle, N., Ardhuin, F., 2009. Drift and mixing under the ocean surface revisited. stratified conditions and model-data comparisons. J. Geophys. Res. 114, C02016. http://dx.doi.org/10.1029/2007JC004466.
Rascle, N., Ardhuin, F., Queffeulou, P., Croizé-Fillon, D., 2008. A global wave parameter database for geophysical applications. Part 1: Wave–current–turbulence interaction parameters for the open ocean based on traditional parameterizations. Ocean Modell. 25, 154–171. http://dx.doi.org/10.1016/j.ocemod.2008.07.006.
Reguero, B.G., Menéndez, M., Méndez, F.J., Mínguez, R., Losada, I.J., 2012. A global ocean wave (GOW) calibrated reanalysis from 1948 onwards. Coastal Eng. 65, 38–55.
Reniers, A.J.H.M., Groenewegen, M.J., Ewans, K.C., Masterton, S., Stelling, G.S., Meek, J., 2010. Estimation of infragravity waves at intermediate water depth. Coastal Eng. 57, 52–61.
Roland, A., 2008. Development of WWM II: Spectral wave modelling on unstructured meshes. Ph.D. thesis, Technische Universität Darmstadt, Institute of Hydraulic and Water Resources Engineering.
Saha, S., Moorthi, S., Pan, H.-L., Wu, X., Wang, J., Nadiga, S., Tripp, P., Kistler, R., Woollen, J., Behringer, D., Liu, H., Stokes, D., Grumbine, R., Gayno, G., Wang, J., Hou, Y.-T., ya Chuang, H., Juang, H.-M.H. a. J.S., Iredell, M., Treadon, R., Kleist, D., Delst, P.V., Keyser, D., Derber, J., Ek, M., Meng, J., Wei, H., Yang, R., Lord, S., van den Dool, H., Kumar, A., Wang, W., Long, C., Chelliah, M., Xue, Y., Huang, B., Schemm, J.-K., Ebisuzaki, W., Lin, R., Xie, P., Chen, M., Zhou, S., Higgins, W., Zou, C.-Z., Liu, Q., Chen, Y., Han, Y., Cucurull, L., Reynolds, R.W., Rutledge, G., Goldberg, M., 2010. The NCEP climate forecast system reanalysis. Bull. Amer. Meterol. Soc. 91, 1015–1057.
Stutzmann, E., Schimmel, M., Ardhuin, F., 2012. Modeling long-term seismic noise in various environments. Geophys. J. Int. 191, 707–722.
Suanez, S., Cariolet, J.-M., Cancouet, R., Ardhuin, F., Delacourt, C., 2012. Dune recovery after storm erosion on a high-energy beach: Vougot Beach, Brittany (France). Geomorphology 139, 16–33.
Sullivan, P.P., McWilliams, J.C., 2010. Dynamics of winds and currents coupled to surface waves. Annu. Rev. Fluid Mech. 42, 19–42.
Tamura, H., Miyazawa, Y., Oey, L.-Y., 2012. The Stokes drift and wave induced-mass flux in the North Pacific. J. Geophys. Res., 117.
Terray, E.A., Donelan, M.A., Agrawal, Y.C., Drennan, W.M., Kahma, K.K., Williams, A.J., Hwang, P.A., Kitaigorodskii, S.A., 1996. Estimates of kinetic energy dissipation under breaking waves. J. Phys. Oceanogr. 26, 792–807.
Tolman, H.L., 2002. Alleviating the garden sprinkler effect in wind wave models. Ocean Modell. 4, 269–289.
Tolman, H.L., 2008. A mosaic approach to wind wave modeling. Ocean Modell. 25, 35–47.
Tolman, H.L., Chalikov, D., 1996. Source terms in a third-generation wind wave model. J. Phys. Oceanogr. 26, 2497–2518. http://journals.ametsoc.org/doi/pdf/10.1175/1520-0485 81996
Tournadre, J., Whitmer, K., Girard-Ardhuin, F., 2008. Iceberg detection in open water by altimeter waveform analysis. J. Geophys. Res. 113 (7), C08040.
Tournadre, J., Girard-Ardhuin, F., Legrsy, B., 2012. Antarctic iceberg distributions 2002–2010. J. Geophys. Res. 117 (7), C05004.
Tran, N., Vandemark, D., Labroue, S., Feng, H., Chapron, B., Tolman, H.L., Lambin, J., Picot, N., 2010. The sea state bias in altimeter sea level estimates determined by combining wave model and satellite data. J. Geophys. Res. 115, C03020.
Vandemark, D., Chapron, B., Sun, J., Crescenti, G.H., Graber, H.C., 2004. Ocean wave slope observations using radar backscatter and laser altimeters. J. Phys. Oceanogr. 34, 2825–2842.
Van Roekel, L.P., Fox-Kemper, B., Sullivan, P.P., Hamlington, P.E., Haney, S.R., 2012. The form and orientation of Langmuir cells for misaligned winds and waves. J. Geophys. Res. 117, C05001.
Wang, W., Huang, R.X., 2004. Wind energy input to the surface waves. J. Phys. Oceanogr. 34, 1276–1280.

Please cite this article in press as: Rascle, N., Ardhuin, F. A global wave parameter database for geophysical applications. Part 2: Model validation with improved source term parameterization. Ocean Modell. (2013), http://dx.doi.org/10.1016/j.ocemod.2012.12.001